



Article

Synthesis of a Rationally Designed Multi-Component Photocatalyst Pt:SiO₂:TiO₂(P25) with Improved Activity for Dye Degradation by Atomic Layer Deposition

Dominik Benz ^{1,*} , Hao Van Bui ^{2,3} , Hubertus T. Hintzen ⁴, Michiel T. Kreutzer ⁵ and J. Ruud van Ommen ^{1,*}

¹ Group Product & Process Engineering, Department of Chemical Engineering, Faculty of Applied Sciences, Delft University of Technology, 2629 HZ Delft, The Netherlands

² Faculty of Electrical and Electronic Engineering, Phenikaa University, Yen Nghia, Ha-Dong District, Hanoi 12116, Vietnam; hao.buivan@phenikaa-uni.edu.vn

³ Phenikaa Research and Technology Institute (PRATI), A&A Green Phoenix Group, 167 Hoang Ngan, Hanoi 10000, Vietnam

⁴ Group Luminescent Materials, Section Fundamental Aspects of Materials and Energy, Faculty of Applied Sciences, Delft University of Technology, 2629 HZ Delft, The Netherlands; h.t.hintzen@tudelft.nl

⁵ Faculty of Science, Leiden University, 2333 CC Leiden, The Netherlands; m.t.kreutzer@science.leidenuniv.nl

* Correspondence: d.benz@tudelft.nl (D.B.); j.r.vanommen@tudelft.nl (J.R.v.O.); Tel.: +31-52782133 (J.R.v.O.)

Received: 5 July 2020; Accepted: 28 July 2020; Published: 30 July 2020



Abstract: Photocatalysts for water purification typically lack efficiency for practical applications. Here we present a multi-component (Pt:SiO₂:TiO₂(P25)) material that was designed using knowledge of reaction mechanisms of mono-modified catalysts (SiO₂:TiO₂, and Pt:TiO₂) combined with the potential of atomic layer deposition (ALD). The deposition of ultrathin SiO₂ layers on TiO₂ nanoparticles, applying ALD in a fluidized bed reactor, demonstrated in earlier studies their beneficial effects for the photocatalytic degradation of organic pollutants due to more acidic surface Si–OH groups which benefit the generation of hydroxyl radicals. Furthermore, our investigation on the role of Pt on TiO₂(P25), as an improved photocatalyst, demonstrated that suppression of charge recombination by oxygen adsorbed on the Pt particles, reacting with the separated electrons to superoxide radicals, acts as an important factor for the catalytic improvement. Combining both materials into the resulting Pt:SiO₂:TiO₂(P25) nanopowder exceeded the dye degradation performance of both the individual SiO₂:TiO₂(P25) (1.5 fold) and Pt:TiO₂(P25) (4-fold) catalysts by 6-fold as compared to TiO₂(P25). This approach thus shows that by understanding the individual materials' behavior and using ALD as an appropriate deposition technique enabling control on the nano-scale, new materials can be designed and developed, further improving the photocatalytic activity. Our research demonstrates that ALD is an attractive technology to synthesize multicomponent catalysts in a precise and scalable way.

Keywords: atomic layer deposition; photocatalysis; dye degradation; TiO₂; multicomponent material

1. Introduction

Titania (TiO₂) was first discovered as an active photocatalyst almost half a century ago [1] and still serves as a widely used benchmark for the development of new photocatalytic materials or as a substrate material to improve their photocatalytic properties [2–4]. The photocatalytic performance combined with affordable price, stability, and non-toxicity are a few reasons for this success in scientific

publications. However, its implementation in real applications, despite these advantages, is hampered by poor sunlight utilization, due to a large bandgap, and charge recombination resulting in insufficient efficiency [5–7]. Improving TiO₂ by incorporating several elements into the lattice (bulk modification) or depositing different materials onto the surface (surface modification) has been extensively explored ever since [8–13]. This includes modifications with both noble metals and metal oxide for the improvement in: (1) reactant adsorption and reactivity by surface modification, (2) light absorption by bandgap modification, (3) charge utilization by modification of the band levels. These three approaches are dominantly targeted to develop a better catalyst. On the other hand, especially improvements in the rates and mechanisms of radical generation are often underestimated since they are often attributed to the improved light absorption or reduced charge recombination. However, it has been shown that surface modifications, which lead to a different type and amount of terminal OH groups, result in an increased OH radical generation [14]. Factors such as adsorption of the reactants for the ROS formation have been demonstrated to play a crucial role in the enhancement of the photocatalytic activity [15–17]. Overall, the photocatalytic mechanism gives four different points to tackle for making improved materials [18,19]:

- (1) Adsorption of reactants.
- (2) Creation of charge carriers by light absorption.
- (3) Charge carrier separation.
- (4) Degradation reactions, along:
 - (a) Conduction band pathway via superoxide radicals (converting into hydroxyl radicals).
 - (b) Valence band pathway via direct oxidation.
 - (c) Valence band pathway via hydroxyl radicals.

While earlier material development focused more on the enhancement using single modifications on active materials, recently, multicomponent systems have received more attention [20–25]. However, most works on multicomponent materials focus on combining materials where components improve the processability of the catalyst for their implementation in future reactors (i.e., dispersion, separation using magnets [21,26]). Multicomponent materials containing iron oxide as a core material, due to its magnetic properties, are good examples of materials improving both the processability and activity of a catalyst to enhance separation from the liquid after the reaction [21,24]. Another approach is to modify the surface of an already photocatalytic material with a coating to change the deposition properties of the subsequently added co-catalyst i.e., increasing control of the particle size by modifying the surface or preventing the agglomeration of deposited nanoclusters of the surface by a cover layer [27–30]. However, the manipulation of physical properties such as increased surface area, the addition of magnetic properties, or a beneficial layer to improve the dispersion of co-catalyst particles [31,32] is more straightforward than modifying the photocatalytic mechanisms themselves. The question arises whether multiple components, each enhancing the photocatalytic process, can be combined to reach higher enhancement than each component individually.

The approach of combining materials to make a more complex and improved structure can be tackled utilizing the advantages of atomic layer deposition. This technology allows to precisely control the deposition of various materials onto a surface. The advantages of confined scalable bottom-up building up of multicomponent catalyst materials could lead to the development of improved photocatalysts. However, building up multicomponent catalysts requires detailed knowledge of the photocatalytic working principles of the base materials as well as the building blocks and their interaction.

Surface deposited Pt on TiO₂(P25) is a well-developed catalyst and has shown superior activity for the photocatalytic degradation of various organic pollutants [33,34]. Pt enhances the photocatalytic activity of TiO₂(P25) for dye degradation by acting as an adsorption surface for O₂ suppressing charge carrier recombination by facilitating improved radical generation via the conduction pathway in the

presence of dissolved O₂ [15,35]. Our previous findings for the role of an ultrathin SiO₂ coating on TiO₂(P25) nanoparticles demonstrated an improved photocatalytic activity due to the improved generation of OH radicals at the SiO₂ surface from the more efficiently separated holes on the SiO₂ surface by the more acidic Si-OH surface groups [14,16], which is different from TiO₂(P25) as well as Pt:TiO₂(P25). From this detailed analysis of the photocatalytic mechanisms, the question arises whether the advantages of these bi-material composites, Pt:TiO₂(P25) and SiO₂:TiO₂(P25), can be combined in a tri-material composite resulting in a further improved photocatalyst for dye degradation. Here, we demonstrate that catalyst development following the design principles of combining characteristics that are improving individual aspects of the photocatalytic reaction pathways can lead to superior photocatalysts by taking advantage of the controllability of the deposition using ALD.

2. Experimental Section

2.1. Synthesis

TiO₂ nanoparticles (P25, mean diameter ~21 nm, specific surface area of ~54 m² g⁻¹ measured by BET) was purchased from Evonik Industries (Hanau, Germany). Silicon tetrachloride (SiCl₄) and trimethyl(methylcyclopentadienyl)platinum(IV) (MeCpPtMe₃) were purchased from AlfaAesar (Karlsruhe, Germany) and Strem Chemicals (Bischheim, France), respectively. Both chemicals were stored in a stainless steel bubbler for mounting into the ALD setup. Acid Blue 9 (Brilliant Blue FCF) and sodium polyphosphate were purchased from SigmaAldrich (Zwijndrecht, The Netherlands) and used without further purification. Pt:SiO₂:TiO₂(P25) was synthesized via a two-step deposition process:

- (1) SiO₂ was deposited on TiO₂(P25) on a homebuilt ALD setup in a fluidized bed under atmospheric pressure, as described in detail elsewhere [36,37]. In brief, 5 g of the TiO₂(P25) powder was put in a quartz glass column (diameter 26 mm, height 500 mm), which was then placed on a vertical vibration table (Paja 40/40-24, Oosterhout, The Netherlands) to assist fluidization. The powder was sieved prior to the ALD experiments with a mesh size of 250 μm to break or exclude larger agglomerates. SiO₂ layers were deposited using SiCl₄ and H₂O as precursors, which were both kept at room temperature in stainless steel bubblers. The reactor was heated to 100 °C throughout the deposition process using an IR lamp. For different SiO₂ loadings, up to 40 cycles were applied using an exposure time of 30 s SiCl₄ and a 3 min H₂O pulse. Purging steps of nitrogen for 3 min and 8 min, respectively, separated the precursor pulses.
- (2) The SiO₂:TiO₂(P25) powder was split into 1.5 g batches, which were then used for the deposition of Pt clusters on the SiO₂:TiO₂(P25) surface using MeCpPtMe₃ and O₂ as precursors. The Pt precursor was stored in stainless steel bubblers and held at 70 °C. For those experiments, one ALD cycle was performed using exposure times for the Pt precursor ranging from 20 sec to 5 min. The O₂ exposure was set to 5 min, and both precursor exposures were separated using purge steps of 5 min with Nitrogen, respectively. Afterward the coated powders were treated under an atmosphere of 5% H₂ in N₂ (*v/v*) in a fixed bed reactor. The temperature was ramped up from room temperature to 200 °C with a rate of 2 °C/min and then was held constant for 5 min after which the powder was allowed to cool to room temperature.

2.2. Characterization

For the ICP-OES analysis, approximately 30 mg of sample was digested in a mixture of 4.5 mL 30% HCl, 1.5 mL 65% HNO₃, and 0.2 mL 40% HF using a microwave for 60 min. After the digestion, the samples were diluted to 50 mL with MilliQ water, and the weight percentage (wt. %) of Pt, Si, and Ti were analyzed with a Perkin Elmer ICP-OES 5300DV (Waltham, MA, USA) system. The samples were also diluted 20 times for the analysis of the Ti concentration. TEM micrographs were acquired from a JEOL JEM1400 transmission electron microscope (Akishima, Japan) at 120 kV. As-deposited Pt:SiO₂:TiO₂(P25) nanoparticles were suspended in ethanol and transferred to Cu transmission electron microscopy grids (3.05 mm in diameter, Quantifoil, Großlobichau, Germany). X-ray photoelectron

spectra (XPS) were recorded on a ThermoFisher K-Alpha (Blijswik, The Netherlands) system using Al K α radiation with a photon energy of 1486.7 eV. A sufficient amount of powders was immobilized on copper tape before loading into the XPS chamber. Survey scans were acquired using a 400 μ m spot size, 55 eV pass energy, and 0.1 eV/step with charge neutralization. The peak positions were calibrated by referencing the C 1s peak to 284.8 eV and previous background subtraction using the Thermo Avantage software (v5.985, accessed on 19 February 2019).

2.3. Photocatalytic Testing

The photocatalytic activity was evaluated in a 100 mL glass bottle (irradiation surface 11.3 cm²) with a 30 mL solution of Acid Blue 9 (16 mg/L in deionized water) and 30 mg of catalyst powder. Sodium polyphosphate (0.3 mL, 100 g/L in water) was added to aid the dispersion of the powder [38]. The powder was dispersed by sonicating the solution with the powder for 10 min. Additionally, the dispersion was stirred in the dark for another 20 min in order to reach the dye-adsorption-desorption equilibrium. The photocatalytic test was executed in open air in an Atlas SunTest XXL (Rycobel, Deerlijk, The Netherlands) solar simulator equipped with three xenon lamps to ensure homogeneous light distribution (top illumination). The irradiance was set to 45 W/m² at the reactor surface with the reactor placed about 40 cm distant from the lamps. In order to ensure a constant temperature during the experiment the reactor was placed in a water bath maintaining a temperature of 20 °C. Multiple samples were irradiated on a multiple stirring plate (700 rpm). Samples of 1 mL were taken after distinct times of irradiation, were subsequently centrifuged, and the dye concentration in the supernatant liquid was determined using a UV/Vis spectrometer (DR5000 Hach-Lange, Düsseldorf, Germany). The absorption was measured at 629 nm, which represents the maximum absorption for Acid Blue 9. Assuming 1st order kinetics, $\ln(C_0/C_t)$ was plotted vs. time, and the slope of the linear regression represents the kinetic constant.

3. Results and Discussion

Previously, we have reported on the mechanisms of SiO₂:TiO₂(P25) [16] and Pt:TiO₂(P25) [35] for the photocatalytic degradation of organic pollutants. With an optimum loading of 1.7 wt. % Si we concluded that for TiO₂(P25), a very thin SiO₂ layer combined improve charge separation with an increased OH radical formation due to more acidic surface OH groups at the SiO₂ surface leading to a higher degradation rate of organic pollutants in water. Too thick an SiO₂ layer shields off the TiO₂ and drastically reduces the photocatalytic activity. For Pt:TiO₂(P25), the role of dissolved O₂ in combination with the enhanced charge separation turned out to be crucial for the enhancement of the photocatalytic activity. Pt acts as a recombination center and reduces the photocatalytic activity if the electrons cannot be harvested adequately in case no O₂ is present or the Pt loading is too high. This gave rise to the improved behavior for Pt:TiO₂(P25) samples with an optimal Pt loading of 0.34 wt. %. Higher loadings decreased the photocatalytic activity even to lower values than intrinsic TiO₂(P25) (>2 wt % Pt). In earlier research, SiO₂ layers often have been used to encapsulate Pt nanoclusters on the surface of TiO₂ to improve the Pt nanoparticle dispersion by preventing noble metal cluster agglomeration, improving the catalytic performance [31,32,39]. According to our previous results, it would be more advantageous to keep Pt clusters exposed on the surface by the deposition of SiO₂ followed by Pt, since both materials, Pt and SiO₂, are crucial for the generation of radicals on the surface. The overcoating of Pt with SiO₂ would reduce the effect of Pt adsorbing O₂ and possibly even give a worse photocatalyst due to the charge recombination property of the Pt nanoclusters in case the lack of access to O₂ prevents the harvest of electrons. Therefore, for the material design, we chose to coat first the TiO₂(P25) nanoparticles with SiO₂ and subsequently deposit Pt onto the SiO₂:TiO₂(P25) substrate (Figure 1a). Despite the spatial separation of the Pt clusters from TiO₂, electrons may still be able to transfer to the Pt clusters as for the SiO₂:TiO₂(P25) catalyst excited electrons may still reach through the ultrathin SiO₂ layer to be harvested [16]. For low Si loadings the layer may be porous and incomplete which would also give the chance for a reaction of the electrons directly on the TiO₂ surface. By applying

2 to 40 ALD cycles of SiCl_4 and H_2O the loading evolved from 0.4 to 2.7 wt % Si in a conformal manner (Figure 1a). Afterward, Pt was deposited onto $\text{SiO}_2\text{:TiO}_2(\text{P25})$ in various loadings by using different pulse times (20 s to 5 min) for MeCpPtMe_3 and O_2 as a counter reactant (Figure 1b). In order to reach the required very low Pt loadings the pulse time was in the undersaturation regime resulting in a dependency of the pulse time versus Pt loading rather the commonly used cycle number. Using this approach, we could precisely tune the loadings for both the SiO_2 coating and the Pt clusters.

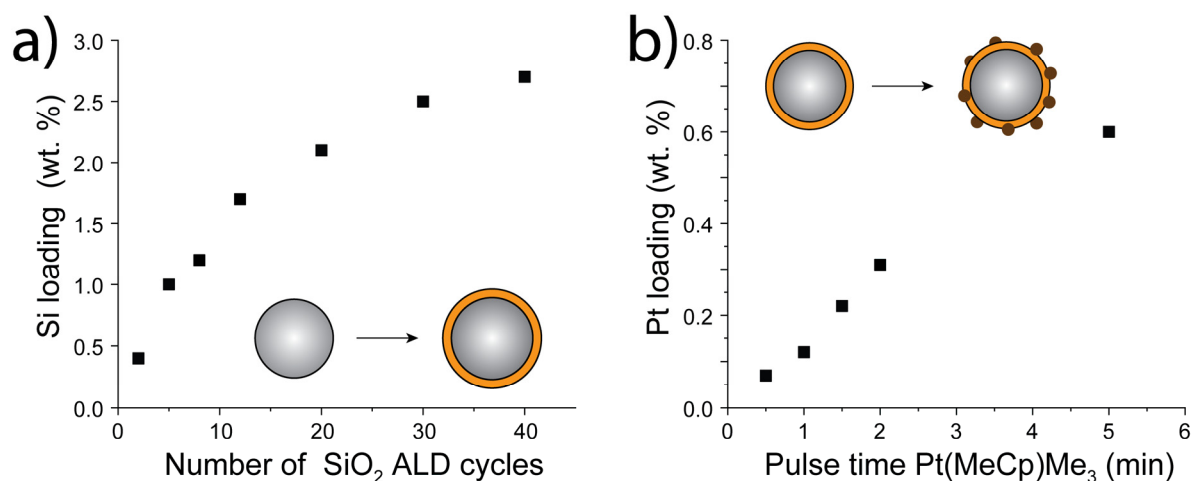


Figure 1. (a) Development of the Si loading with the number of applied SiO_2 ALD cycles on $\text{TiO}_2(\text{P25})$ particles, (b) Development of the Pt loading with the Pt precursor pulse time (MeCpPtMe_3) on SiO_2 coated $\text{TiO}_2(\text{P25})$ particles (2.1 ± 0.2 wt. % Si).

This design of experiments gives a matrix of various combinations of SiO_2 and Pt loadings onto P25 nanoparticles. Analyzing the morphology with TEM revealed the growth of SiO_2 as conformal sub-nanometer layers layers with various loading (Figure 2a) onto P25 and the Pt clusters (1–2 nm) deposited onto the SiO_2 layers in the second step (Figure 2b, Figure S1). This is in agreement with our previous studies that show the growth of layers of SiO_2 due to the high affinity towards the TiO_2 surface [17]. On the other hand, the high surface energy of Pt results in the expected island growth on the surface of SiO_2 , resulting in similar behavior as the deposition of Pt clusters on P25 itself [40]. Due to the very minute addition of material on the P25 particles TEM pictures confirms an unchanged particle size of $\text{Pt:SiO}_2\text{:TiO}_2(\text{P25})$ particles compared to pristine P25 of about 30 nm (Figure 2b). For lower loaded SiO_2 samples, the layers are not clearly visible due to resolution limitations of the TEM. It is expected that for a low number of cycles, the SiO_2 layer may be incomplete, and the TiO_2 surface is still exposed. XPS confirmed the deposition of both materials, SiO_2 and Pt (Figure 2c–e). From the high-resolution spectra, we can identify the characteristic peaks for each element – Ti, Si, and Pt. For the range between 450 eV and 475 eV, the characteristic Ti(IV) peaks for TiO_2 can be observed at binding energies of 458.68 eV (Ti $2p_{3/2}$) and 464.34 eV (Ti $2p_{1/2}$). The Si 2p peak characteristic for SiO_2 arises at 102.36 eV. After deconvolution of the Pt HR-XPS spectrum, three peaks arise where the peaks at 70.90 eV and 74.01 eV can be fitted to Pt(0) $4f_{7/2}$ and Pt(0) $4f_{5/2}$ respectively correlating them to the metallic Pt species, and at a binding energy of 76.06 eV, a satellite peak from the Ti 3s peak arises. XRD studies on $\text{TiO}_2(\text{P25})$ after modification with SiO_2 and Pt using ALD showed no change in the TiO_2 crystal structure featuring anatase and rutile phase typical for the mixed phase P25 nanoparticles (Figure S3). The modified $\text{TiO}_2(\text{P25})$ showed a peak at 46.6° indicating the Pt(200) facet. However, other facets of Pt were not observable. Due to the only minute changes, i.e., ultra-thin layers of SiO_2 on the surface of TiO_2 XRD features of SiO_2 remain undetected. UV/Vis absorbance spectra (measured with DRS) show that the addition of neither SiO_2 layers nor Pt clusters leads to a significant change in the bandgap of the modified catalysts (Figure S4). The deposition of Pt clusters leads (for both $\text{TiO}_2(\text{P25})$ itself as well as $\text{SiO}_2\text{:TiO}_2(\text{P25})$) to strong absorption throughout the visible

spectrum caused by the metallic particles on the surface of the catalysts. Previous studies on the effect of the BET surface area of the single modified materials $\text{SiO}_2\text{:TiO}_2(\text{P25})$ ($54 \text{ m}^2/\text{g}$) [17] and $\text{Pt:TiO}_2(\text{P25})$ ($55 \text{ m}^2/\text{g}$) [35] demonstrated that a minute additions of SiO_2 and Pt are not significantly affecting the BET surface area compared to pure $\text{TiO}_2(\text{P25})$ ($55 \text{ m}^2/\text{g}$). Therefore we expect a similar BET surface area for the bi-modified $\text{Pt:SiO}_2\text{:TiO}_2(\text{P25})$ photocatalyst. Furthermore, the adsorption of Acid Blue 9 on the surface of the prepared catalysts after reaching the adsorption-desorption equilibrium did not change significantly upon modification of $\text{TiO}_2(\text{P25})$ (Figure S5).

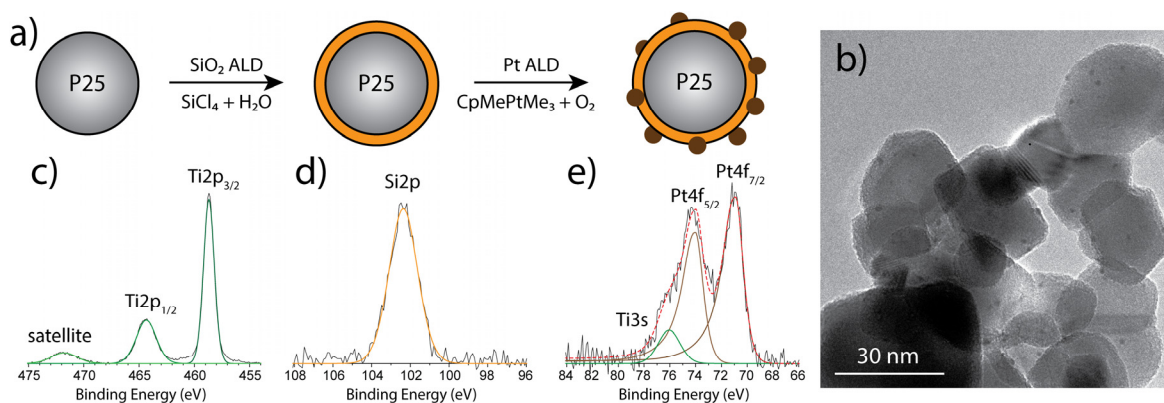


Figure 2. (a) Deposition scheme for the material development of $\text{Pt:SiO}_2\text{:TiO}_2(\text{P25})$, (b) TEM picture of $\text{Pt:SiO}_2\text{:TiO}_2(\text{P25})$ (1 wt. % Si, 1.23 wt. % Pt), grey large particle are P25 particles, SiO_2 layer around P25 particles can be observed, dark spots indicate Pt nanoclusters, (c) Ti 2p HRXPS spectrum with typical TiO_2 features, (d) Si 2p HRXPS spectrum, single peak represents SiO_2 (orange), (e) Pt 4f HRXPS spectrum, doublet peak represents Pt metal (brown), single peak represents Ti 3s satellite peak (green).

In order to investigate the photocatalytic performance of the combined material ($\text{Pt:SiO}_2\text{:TiO}_2(\text{P25})$), it is compared to the original material ($\text{TiO}_2(\text{P25})$) and the single-modified materials – $\text{Pt:TiO}_2(\text{P25})$ and $\text{SiO}_2\text{:TiO}_2(\text{P25})$. First, the photocatalytic degradation for those individual compounds is investigated to benchmark the measurements. As compared to $\text{TiO}_2(\text{P25})$, the optimal Pt loading of about 0.34 wt. % gives a 4-fold increase in the activity of $\text{Pt:TiO}_2(\text{P25})$ for the photocatalytic degradation of AB9 (Figure 3a) while $\text{SiO}_2\text{:TiO}_2(\text{P25})$ shows a 1.5-fold increased photocatalytic activity with an optimal loading of about 1.2 wt. % Si (Figure 3b). In our previous research, an optimal loading of about 1.8 wt. % Si was reported, which is in line with the results in this paper [16].

In Figure 3, we show the photocatalytic degradation of Acid Blue 9 for different coated $\text{Pt:SiO}_2\text{:TiO}_2(\text{P25})$ samples with various SiO_2 and Pt loading in order to find the optimum loading. We can identify an optimal behavior in the range of 1.5–2.2 wt. % Si and around 0.3–0.4 wt. % Pt (Figure 3c). This range is also covering the ranges of individual catalysts $\text{SiO}_2\text{:TiO}_2(\text{P25})$ and $\text{Pt:TiO}_2(\text{P25})$ perform in an optimal way. The best performing catalyst of the $\text{Pt:SiO}_2\text{:TiO}_2(\text{P25})$ series (1.9 wt. % Si, 0.60 wt. % Pt) degrades AB9 about six times better than P25. Evidently, the combination of Pt nanoparticles onto sub-nanometer layers of SiO_2 coated on P25 particles results in an improved photocatalytic material. Although the best performing catalyst with 0.60 wt. % Pt is slightly outside the range of the optimal loading (Table 1, Figure S2) for $\text{Pt:TiO}_2(\text{P25})$ mono-modified (0.34 wt. %), the fitting of the data (2D polynomial model) reveals that the optimal loading for the mono-modified materials $\text{Pt:TiO}_2(\text{P25})$ and $\text{SiO}_2\text{:TiO}_2(\text{P25})$ coincides with the optimal loadings for these mono-modified catalysts. This indicates that there is limited interaction between the improvement mechanisms of depositing SiO_2 and Pt onto P25. In this context it may be speculated that the growth of Pt on the SiO_2 coating may positively influence particle size distribution due to a change in surface energy. However, a study on the detailed evolution of the particle size distribution of Pt clusters on different surfaces would be outside of the scope of this study yet important for further research.

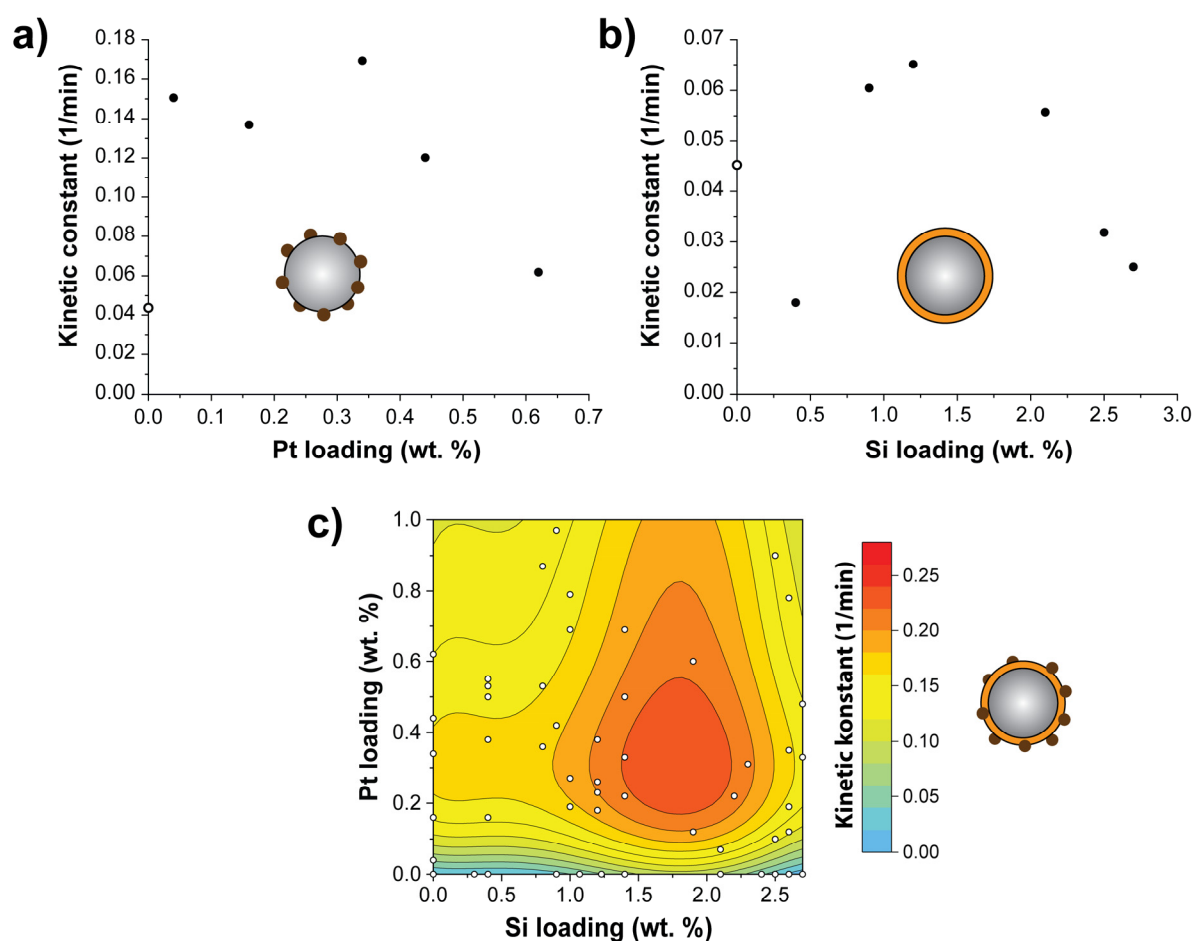


Figure 3. Kinetic constant for degradation of AB9 (a) with different loadings of Pt on TiO₂(P25), (b) with different loadings of SiO₂ on TiO₂(P25), (c) combined Pt:SiO₂:TiO₂(P25) material with different loadings of Pt and Si (fitted results, see also Figure S2).

Table 1. Kinetic constants for the best performing photocatalysts for the mono-modified and bi-modified TiO₂ catalysts. Kinetic constants are calculated from pseudo 1st order kinetics.

	P25	Pt:TiO ₂ (P25)	SiO ₂ :TiO ₂ (P25)	Pt:SiO ₂ :TiO ₂ (P25)
Optimal Loading	–	0.34 wt. % (Pt)	1.2 wt. % (Si)	0.6 wt. % (Pt) 1.9 wt. % (Si)
Kinetic Constant (min ⁻¹)	0.044	0.169	0.065	0.267
Improvement Ratio	1	3.84	1.48	6.07

On the one hand, a sub-nanometer SiO₂ layer on TiO₂(P25) particles improves the OH radical generation at the SiO₂ surface from the holes generated in the VB. On the other hand, Pt clusters facilitate effective electron-hole-pair separation by using the TiO₂ CB electrons as reducing agents to generate superoxide radicals (O₂⁻) from dissolved O₂. Combining both materials, SiO₂ and Pt, with TiO₂(P25) increases the photocatalytic activity by increasing mainly the radical generation.

The current study does not show any serious deactivation of the photocatalyst during the use of the photocatalyst. Nevertheless, a detailed analysis of the long-term reusability will be required for the implementation in future reactors for water treatment and is recommended to be subject to follow-up research. Applying the same strategy followed in this research to improve the photocatalytic activity using a base material with increased light absorption could further increase the overall performance. For example, N-doping has been shown to reduce the bandgap of titania, increasing the light absorption

in the visible light regime [41,42]. Adding another material on the surface is, on the other hand, not recommended. This would probably lead to coverage of the photocatalytic relevant surface groups reducing the reactive oxygen species generation. Furthermore, the modification of TiO₂ by layer/nanocluster combination using cheaper materials as replacement for e.g., Pt may result in both efficient and cheaper catalysts. In our experiments we were able to coat powder of up to 5 g (~270 m² surface area) using atomic layer deposition in a fluidized bed. This technique provides therefore a great opportunity to scale up the preparation of multicomponent catalysts.

4. Conclusions

This work shows that by the smart combination of different materials onto TiO₂(P25), better photocatalyst can be engineered using the excellent precision of ALD in a fluidized bed. As a successful example we designed a Pt:SiO₂:TiO₂(P25) material with improved photocatalytic properties by depositing Pt clusters on SiO₂ coated TiO₂(P25). The choice of the coating materials Pt and SiO₂ was based on our previous detailed analysis of the photocatalytic mechanism of both SiO₂:TiO₂(P25) and Pt:TiO₂(P25). ALD provided the opportunity to precisely control the loading of SiO₂ and Pt, resulting in a matrix of various loaded Pt:SiO₂:TiO₂(P25) surface modified nanoparticles. We showed that this material accelerates the photocatalytic degradation rate of Acid Blue 9 by a factor 6, which is superior to both SiO₂:TiO₂(P25) (1.5×) and Pt:TiO₂(P25) (4×).

Supplementary Materials: The following are available online at <http://www.mdpi.com/2079-4991/10/8/1496/s1>, Figure S1: TEM pictures of Pt:P25 and SiO₂:25, Figure S2: raw data photocatalytic activity, Figure S3: XRD spectra, Figure S4: UV/Vis DRS spectra, Figure S5: dye adsorption on catalyst surface.

Author Contributions: Conceptualization, D.B., H.V.B., H.T.H. and J.R.v.O.; methodology, D.B.; validation, D.B.; formal analysis, D.B.; investigation, D.B.; resources, J.R.v.O.; data curation, J.R.v.O.; writing—original draft preparation, D.B.; writing—review and editing, D.B., H.V.B., H.T.H., J.R.v.O., M.T.K.; visualization, D.B.; supervision, H.V.B., H.T.H., J.R.v.O. and M.T.K.; project administration, J.R.v.O.; funding acquisition, H.V.B. and J.R.v.O. All authors have read and agreed to the published version of the manuscript.

Funding: This research is supported by the TU Delft | Global Initiative, a program of the Delft University of Technology to boost Science and Technology for Global Development.

Conflicts of Interest: The authors declare no conflict of interest.

References

1. Fujishima, A.; Honda, K. Electrochemical Photolysis of Water at a Semiconductor Electrode. *Nature* **1972**, *238*, 37–38. [[CrossRef](#)] [[PubMed](#)]
2. Pastrana-Martínez, L.M.; Morales-Torres, S.; Carabineiro, S.A.; Buijnsters, J.G.; Figueiredo, J.L.; Silva, A.M.; Faria, J.L. Photocatalytic activity of functionalized nanodiamond-TiO₂ composites towards water pollutants degradation under UV/Vis irradiation. *Appl. Surf. Sci.* **2018**, *458*, 839–848. [[CrossRef](#)]
3. Driessen, M.D.; Grassian, V.H. Photooxidation of Trichloroethylene on Pt/TiO₂. *J. Phys. Chem. B* **1998**, *102*, 1418–1423. [[CrossRef](#)]
4. Wang, M.; Sun, L.; Lin, Z.; Cai, J.; Xie, K.; Lin, C. p–n Heterojunction photoelectrodes composed of Cu₂O-loaded TiO₂ nanotube arrays with enhanced photoelectrochemical and photoelectrocatalytic activities. *Energy Environ. Sci.* **2013**, *6*, 1211. [[CrossRef](#)]
5. Ahmed, S.; Rasul, M.G.; Martens, W.N.; Brown, R.; Hashib, M.A. Advances in Heterogeneous Photocatalytic Degradation of Phenols and Dyes in Wastewater: A Review. *Water Air Soil Pollut.* **2010**, *215*, 3–29. [[CrossRef](#)]
6. Pelaez, M.; Nolan, N.T.; Pillai, S.C.; Seery, M.K.; Falaras, P.; Kontos, A.G.; Dunlop, P.; Hamilton, J.; Byrne, J.A.; O’Shea, K.; et al. A review on the visible light active titanium dioxide photocatalysts for environmental applications. *Appl. Catal. B* **2012**, *125*, 331–349. [[CrossRef](#)]
7. Anwer, H.; Mahmood, A.; Lee, J.; Kim, K.-H.; Park, J.-W.; Yip, A.C.K. Photocatalysts for degradation of dyes in industrial effluents: Opportunities and challenges. *Nano Res.* **2019**, *12*, 955–972. [[CrossRef](#)]
8. Carneiro, J.T.; Savenije, T.J.; Moulijn, J.A.; Mul, G. The effect of Au on TiO₂ catalyzed selective photocatalytic oxidation of cyclohexane. *J. Photochem. Photobiol. A* **2011**, *217*, 326–332. [[CrossRef](#)]

9. Lim, T.H.; Jeong, S.M.; Kim, S.D.; Gyenis, J. Degradation characteristics of NO by photocatalysis with TiO₂ and CuO/TiO₂. *React. Kinet. Catal. Lett.* **2000**, *71*, 223–229. [[CrossRef](#)]
10. Lei, M.; Wang, N.; Zhu, L.H.; Zhou, Q.L.; Nie, G.; Tang, H.Q. Photocatalytic reductive degradation of polybrominated diphenyl ethers on CuO/TiO₂ nanocomposites: A mechanism based on the switching of photocatalytic reduction potential being controlled by the valence state of copper. *Appl. Catal. B Environ.* **2016**, *182*, 414–423. [[CrossRef](#)]
11. Gong, Y.; Wang, D.P.; Wu, R.; Gazi, S.; Soo, H.S.; Sritharan, T.; Chen, Z. New insights into the photocatalytic activity of 3-D core-shell P25@silica nanocomposites: Impact of mesoporous coating. *Dalton Trans.* **2017**, *46*, 4994–5002. [[CrossRef](#)] [[PubMed](#)]
12. Tsukamoto, D.; Shiraiishi, Y.; Sugano, Y.; Ichikawa, S.; Tanaka, S.; Hirai, T. Gold Nanoparticles Located at the Interface of Anatase/Rutile TiO₂ Particles as Active Plasmonic Photocatalysts for Aerobic Oxidation. *J. Am. Chem. Soc.* **2012**, *134*, 6309–6315. [[CrossRef](#)] [[PubMed](#)]
13. Zhou, Y.; King, D.M.; Liang, X.; Li, J.; Weimer, A.W. Optimal preparation of Pt/TiO₂ photocatalysts using atomic layer deposition. *Appl. Catal. B* **2010**, *101*, 54–60. [[CrossRef](#)]
14. Simonsen, M.E.; Li, Z.; Sogaard, E.G. Influence of the OH groups on the photocatalytic activity and photoinduced hydrophilicity of microwave assisted sol-gel TiO₂ film. *Appl. Surf. Sci.* **2009**, *255*, 8054–8062. [[CrossRef](#)]
15. Muhich, C.L.; Zhou, Y.; Holder, A.M.; Weimer, A.W.; Musgrave, C.B. Effect of Surface Deposited Pt on the Photoactivity of TiO₂. *J. Phys. Chem. C* **2012**, *116*, 10138–10149. [[CrossRef](#)]
16. Benz, D.; Bui, H.V.; Hintzen, H.T.; Kreutzer, M.T.; Van Ommen, J.R. Mechanistic insight into the improved photocatalytic degradation of dyes using TiO₂(P25) nanoparticles with an ultrathin SiO₂ coating. In press.
17. Guo, J.; Benz, D.; Nguyen, T.-T.D.; Nguyen, P.-H.; Le, T.-L.T.; Nguyen, H.-H.; La Zara, D.; Liang, B.; Hintzen, H.B.; Van Ommen, J.R.; et al. Tuning the Photocatalytic Activity of TiO₂ Nanoparticles by Ultrathin SiO₂ Films Grown by Low-Temperature Atmospheric Pressure Atomic Layer Deposition. *Appl. Surf. Sci.* **2020**, *530*, 147244. [[CrossRef](#)]
18. Gaya, U.I. Mechanistic Principles of Photocatalytic Reaction. In *Heterogeneous Photocatalysis Using Inorganic Semiconductor Solids*; Gaya, U.I., Ed.; Springer: Dordrecht, The Netherlands, 2014; pp. 73–89.
19. Linsebigler, A.L.; Lu, G.; Yates, J.T. Photocatalysis on TiO₂ Surfaces: Principles, Mechanisms, and Selected Results. *Chem. Rev.* **1995**, *95*, 735–758. [[CrossRef](#)]
20. Zhang, A.-Y.; Wang, W.-K.; Pei, D.-N.; Yu, H.-Q. Degradation of refractory pollutants under solar light irradiation by a robust and self-protected ZnO/CdS/TiO₂ hybrid photocatalyst. *Water Res.* **2016**, *92*, 78–86.
21. Yu, X.; Liu, S.; Yu, J. Superparamagnetic γ -Fe₂O₃@SiO₂@TiO₂ composite microspheres with superior photocatalytic properties. *Appl. Catal. B* **2011**, *104*, 12–20. [[CrossRef](#)]
22. Zhang, F.; Liu, W.; Liu, Y.; Wang, J.; Ji, G. Fabrication and enhanced photocatalytic properties of Pt@SiO₂@TiO₂ composites by surface plasma resonance from Pt nanoparticles. *J. Nanopart. Res.* **2015**, *17*, 62. [[CrossRef](#)]
23. Li, S.-X.; Cai, J.; Wu, X.; Liu, B.; Chen, Q.; Li, Y.; Zheng, F. TiO₂@Pt@CeO₂ nanocomposite as a bifunctional catalyst for enhancing photo-reduction of Cr (VI) and photo-oxidation of benzyl alcohol. *J. Hazard. Mater.* **2018**, *346*, 52–61. [[CrossRef](#)] [[PubMed](#)]
24. Deng, X.; Li, S. Vapor phase synthesis of 2,3,6-trimethylphenol from m-cresol and methanol with Fe₂O₃-SiO₂-CuO catalyst. *Catal. Commun.* **2018**, *111*, 100–103. [[CrossRef](#)]
25. Wang, J.; Kondrat, S.; Wang, Y.; Brett, G.L.; Giles, C.; Bartley, J.K.; Lu, L.; Liu, Q.; Kiely, C.J.; Hutchings, G.J. Au-Pd Nanoparticles Dispersed on Composite Titania/Graphene Oxide-Supports as a Highly Active Oxidation Catalyst. *ACS Catal.* **2015**, *5*, 3575–3587. [[CrossRef](#)]
26. Liu, S.; Guo, M.-X.; Shao, F.; Peng, Y.-H.; Bian, S.-W. Water-dispersible and magnetically recoverable Fe₃O₄/Pd@nitrogen-doped carbon composite catalysts for the catalytic reduction of 4-nitrophenol. *RSC Adv.* **2016**, *6*, 76128–76131. [[CrossRef](#)]
27. Cheng, N.; Banis, M.N.; Liu, J.; Riese, A.; Li, X.; Li, R.; Ye, S.; Knights, S.; Sun, X. Extremely Stable Platinum Nanoparticles Encapsulated in a Zirconia Nanocage by Area-Selective Atomic Layer Deposition for the Oxygen Reduction Reaction. *Adv. Mater.* **2015**, *27*, 277–281. [[CrossRef](#)]
28. Dai, Y.; Zhu, M.; Wang, X.; Wu, Y.; Huang, C.; Fu, W.; Meng, X.; Sun, Y. Visible-light promoted catalytic activity of dumbbell-like Au nanorods supported on graphene/TiO₂ sheets towards hydrogenation reaction. *Nanotechnology* **2018**, *29*, 245703. [[CrossRef](#)]

29. Bo, Z.; Ahn, S.; Ardagh, M.A.; Schweitzer, N.M.; Canlas, C.P.; Farha, O.K.; Notestein, J.M.; Farh, O.K. Synthesis and stabilization of small Pt nanoparticles on TiO₂ partially masked by SiO₂. *Appl. Catal. A* **2018**, *551*, 122–128. [[CrossRef](#)]
30. Song, Z.; Wang, B.; Cheng, N.; Yang, L.; Banham, D.; Li, R.; Ye, S.; Sun, X. Atomic layer deposited tantalum oxide to anchor Pt/C for a highly stable catalyst in PEMFCs. *J. Mater. Chem. A* **2017**, *5*, 9760–9767. [[CrossRef](#)]
31. Wan, C.; Cheng, D.G.; Chen, F.; Zhan, X. Fabrication of CeO₂ nanotube supported Pt catalyst encapsulated with silica for high and stable performance. *Chem. Commun.* **2015**, *51*, 9785–9788. [[CrossRef](#)]
32. Zhao, E.W.; Maligal-Ganesh, R.V.; Mentink-Vigier, F.; Zhao, T.Y.; Du, Y.; Pei, Y.; Huang, W.; Bowers, C.R. Atomic-Scale Structure of Mesoporous Silica-Encapsulated Pt and PtSn Nanoparticles Revealed by Dynamic Nuclear Polarization-Enhanced ²⁹Si MAS NMR Spectroscopy. *J. Phys. Chem. C* **2019**, *123*, 7299–7307. [[CrossRef](#)]
33. Sadeghi, M.; Liu, W.; Zhang, T.G.; Stavropoulos, P.; Levy, B. Role of Photoinduced Charge Carrier Separation Distance in Heterogeneous Photocatalysis: Oxidative Degradation of CH₃OH Vapor in Contact with Pt/TiO₂ and Cofumed TiO₂-Fe₂O₃. *J. Phys. Chem.* **1996**, *100*, 19466–19474. [[CrossRef](#)]
34. Chen, J.-J.; Wang, W.-K.; Li, W.-W.; Pei, D.-N.; Yu, H.-Q. Roles of Crystal Surface in Pt-Loaded Titania for Photocatalytic Conversion of Organic Pollutants: A First-Principle Theoretical Calculation. *ACS Appl. Mater. Interfaces* **2015**, *7*, 12671–12678. [[CrossRef](#)] [[PubMed](#)]
35. Benz, D.; Felter, K.M.; Köser, J.; Thöming, J.; Mul, G.; Grozema, F.C.; Hintzen, H.T.; Kreutzer, M.T.; van Ommen, J.R. Assessing the Role of Pt Clusters on TiO₂(P25) on the Photocatalytic Degradation of Acid Blue 9 and Rhodamine B. *J. Phys. Chem. C* **2020**, *124*, 8269–8278. [[CrossRef](#)]
36. Beetstra, R.; Lafont, U.; Nijenhuis, J.; Kelder, E.M.; van Ommen, J.R. Atmospheric Pressure Process for Coating Particles Using Atomic Layer Deposition. *Chem. Vap. Depos.* **2009**, *15*, 227–233. [[CrossRef](#)]
37. van Ommen, J.R.; Goulas, A. Atomic layer deposition on particulate materials. *Mater. Today Chem.* **2019**, *14*, 100183. [[CrossRef](#)]
38. van Driel, B.A.; Kooyman, P.J.; van den Berg, K.J.; Schmidt-Ott, A.; Dik, J. A quick assessment of the photocatalytic activity of TiO₂ pigments—From lab to conservation studio! *Microchem. J.* **2016**, *126*, 162–171. [[CrossRef](#)]
39. Shan, J.; Lei, Z.; Wu, W.; Tan, Y.; Cheng, N.; Sun, X. Highly Active and Durable Ultrasmall Pd Nanocatalyst Encapsulated in Ultrathin Silica Layers by Selective Deposition for Formic Acid Oxidation. *ACS Appl. Mater. Interfaces* **2019**, *11*, 43130–43137. [[CrossRef](#)]
40. Faust, M.; Enders, M.; Gao, K.; Reichenbach, L.; Muller, T.; Gerlinger, W.; Sachweh, B.; Kasper, G.; Bruns, M.; Bräse, S.; et al. Synthesis of Pt/SiO₂ Catalyst Nanoparticles from a Continuous Aerosol Process using Novel Cyclo-octadienylplatinum Precursors. *Chem. Vap. Depos.* **2013**, *19*, 274–283. [[CrossRef](#)]
41. Gao, B.; Ma, Y.; Cao, Y.; Yang, W.; Yao, J. Great Enhancement of Photocatalytic Activity of Nitrogen-Doped Titania by Coupling with Tungsten Oxide. *J. Phys. Chem. B* **2006**, *110*, 14391–14397. [[CrossRef](#)]
42. Zhang, J.; Wu, Y.; Xing, M.; Leghari, S.A.K.; Sajjad, S. Development of modified N doped TiO₂ photocatalyst with metals, nonmetals and metal oxides. *Energy Environ. Sci.* **2010**, *3*, 715–726. [[CrossRef](#)]

